APPLIED ORGANOMETALLIC CHEMISTRY
Appl. Organometal. Chem. 2001; **15**: 858–866
DOI: 10.1002/aoc.243

Thermal stability of SiCN ceramics studied by spectroscopy and electron microscopy

H.-J. Kleebe,* H. Störmer, S. Trassl and G. Ziegler
Institute for Materials Research (IMA I), University of Bayreuth, D-95440 Bayreuth, Germany

Processing of two precursor-derived SiCN ceramic monoliths was performed employing different liquid polymers, which were obtained by ammonolysis of functionalized chlorosilanes. Preparation of monolithic samples was performed by mixing liquid polysilazane with cross-linked SiCN-powder particles, derived from the same precursors by heat treatment at 300 °C, and subsequent annealing upon pyrolysis at temperatures exceeding 1000 °C to initiate crystallization. Characterization of the polymer-derived ceramics was performed after pyrolysis at 1000 °C and, in particular, after annealing at temperatures ranging from 1400 to 1540 °C. Transmission electron microscopy was conducted in order to study the devitrification/thermal stability of the corresponding bulk SiCN glasses. Depending on the functionalities of the SiCN precursor and the processing conditions, different microstructures were obtained. The material prepared from precursor A showed crystallization of large α-Si_3N_4 grains within the overall homogeneous amorphous bulk material after exposure at 1540 °C for 6 h in nitrogen atmosphere. In contrast, the ceramic monoliths derived from SiCN precursor B remained completely amorphous, with no indication of local nucleation or crystallization. It is thought that devitrification of these polymer-derived glasses is promoted by local rearrangements of the glass network within the amorphous bulk. In addition, the role of the excess free carbon, commonly present in polymer-derived SiCN ceramics, on the thermal stability is discussed. Copyright © 2001 John Wiley & Sons, Ltd.

Keywords: thermal stability; ceramic; SiCN; polymer

* Correspondence to: H.-J. Kleebe, Colorado School of Mines, Metallurgical & Materials Engineering Dept., Golden, CO 80401, USA.
E-mail: hkleebe@mines.edu
Contract/grant sponsor: Volkswagenstiftung Hannover.
Contract/grant sponsor: Deutsche Forschungsgemeinschaft.

Received 18 April 2000; accepted 30 October 2000

1 INTRODUCTION

In recent years, the need for advanced materials, which can be utilized under severe service conditions, directed worldwide research activities towards the fabrication of non-oxide ceramics like BN, B_4C, SiC, Si_3N_4 or composites thereof. Since Verbeek and Winter[1] and Yajima *et al.*[2] succeeded in the mid 1970s in obtaining SiCN and SiC fibers from organosilicon polymers, it is now well established that these ceramics can also be produced by thermal degradation of appropriate organosilicon preceramic compounds, yielding silicon-based non-oxide ceramics at quite low temperatures. This finding resulted in extensive studies on the synthesis of numerous polymeric precursors that can be transformed into non-oxide ceramics.[3–12] Apart from synthesis, the potential to utilize organometallic compounds for the preparation of powders, binders, fibers, coatings, infiltration of porous matrices, and the fabrication of bulk materials has been investigated intensively.[13–23] The most attractive feature of the polymer pyrolysis process, compared with conventional powder-metallurgical methods, is the low processing temperature, since the precursors can be transformed into ceramic components at temperatures as low as 800–1000 °C; there is also the advantage of the applicability of established polymer-processing techniques. Polymer pyrolysis allows the realization of materials with high purity, because the elements that compose the final ceramic are already bonded to each other on an atomic level within the starting precursor.

Generally, processing of ceramic materials *via* organometallic compounds involves: (i) the synthesis of the precursor on the basis of monomer units, followed by (ii) cross-linking into an unmeltable (with the exception of fiber processing), three-dimensional polymer network, enabling high cera-

mic yield and shape stability upon (iii) subsequent pyrolysis in the temperature range between 800 and 1000 °C. Pyrolysis initiates the organic–inorganic transition, yielding an amorphous, non-oxide covalent glass. Further heat treatment at temperatures exceeding 1000 °C promotes crystallization of the thermodynamically stable phases and results in a partially or entirely crystallized material.

To exploit the full potential of these polymer ceramics, comprehensive knowledge of the effect of polymer architecture on the ceramization mechanism during pyrolysis, and on the final microstructure after amorphous/crystalline transformation is required. Several studies reported in literature have been devoted to the synthesis of new organometallic compounds with different functional groups and their transformation into amorphous ceramic residues.[24–34] Commonly, investigations in this area of research focus on the pyrolysis behavior of polymeric precursors, but they do not include the study of their specific devitrification behavior. Up to now, little understanding has been developed concerning the problem of thermal degradation/crystallization of these glasses. One of the main goals, however, is the retention of the amorphous state up to high temperatures. Only when the material remains amorphous under service conditions, no marked change in mechanical/electrical properties is expected to occur.[35–38]

Transmission electron microscopy (TEM) investigations by Monthioux and coworkers[35,39] focused on the crystallization phenomena observed in different Si–C, Si–C–N, Si–C–O and Si–C–N–O glasses. They proposed that the free carbon phase, commonly present in amorphous polymer-derived materials, is the first phase to nucleate as so-called basic structural units (BSUs), followed by the crystallization of SiC. Kleebe and coworkers[40,41] reported on the microstructure development of monolithic SiCN-based glasses. They showed that, depending on the pre-annealing temperature of polymer-derived powder particles used for materials synthesis, different microstructures were obtained. It is interesting to note that high-temperature annealing of the polymer particles used resulted in the crystallization of the surrounding matrix; the particles, however, remained amorphous.[41] It was concluded that nanosized porosity within the binder phase initiated local SiC crystallization. Bill and Aldinger[42] studied the quaternary system Si–B–C–N and indicated a higher thermal stability with respect to crystallization compared with SiCN ceramics. In addition, they showed that, when adding a supplement element to the ternary Si–C–N system, the microstructure can be altered. Whereas the addition of phosphorus results in a rather coarse microstructure, with SiC and Si_3N_4 being several micrometers in diameter, the addition of boron favors the formation of a fine-grained microstructure with both constituents being only a few tens of nanometers in size. It was concluded that, in the latter case, thin B(C)N coatings at phase boundaries acted as a diffusion barrier retarding SiC and Si_3N_4 grain growth.

The intention of this work was to study the thermal stability of bulk SiCN ceramics, derived from two different precursors. Since local crystallization phenomena are of utmost importance in understanding the amorphous to crystalline transition in general, TEM in combination with electron energy-loss spectroscopy (EELS) was employed as the main characterization tool. Characterization of polymer-derived ceramics *via* TEM particularly advantageous, on account of being able to: (i) study the microstructure and microchemistry with a high spatial resolution; (ii) make an unequivocal distinction between the amorphous and crystalline state of the region of interest.[43]

2 EXPERIMENTAL PROCEDURES

All preparation steps for the fabrication of SiCN monoliths were carried out in an inert gas atmosphere owing to the air and moisture sensitivity of both educts and products. Synthesis followed standard procedures,[7] i.e. dissolving of different di- and tri-functionalized chlorosilanes in toluene and passing ammonia through the solution. Subsequent filtration of the ammonium chloride from the reaction mixture and distillation of the solvent leads to colorless or pale yellow silazane precursors.

Two different polyvinylsilazanes with the nominal formula $[(NH)SiCH_3CH{=}CH_2]_x$ $[(NH)SiHCH_3]_y$ (precursor A, (HPS)) and $[(NH)_{1.5}SiCH{=}CH_2]_x$ (precursor B, (TVS)) were employed for sample preparation. After synthesis, the liquid precursor was first converted into an unmeltable crosslinked polymer by thermal treatment at 300 °C for 3 h. The thermal curing was catalytically supported by adding 1 wt% of dicumylperoxide, which initiates polymerization of the functional vinyl groups and reduces the evolution of low molecular mass oligomeric silazanes.

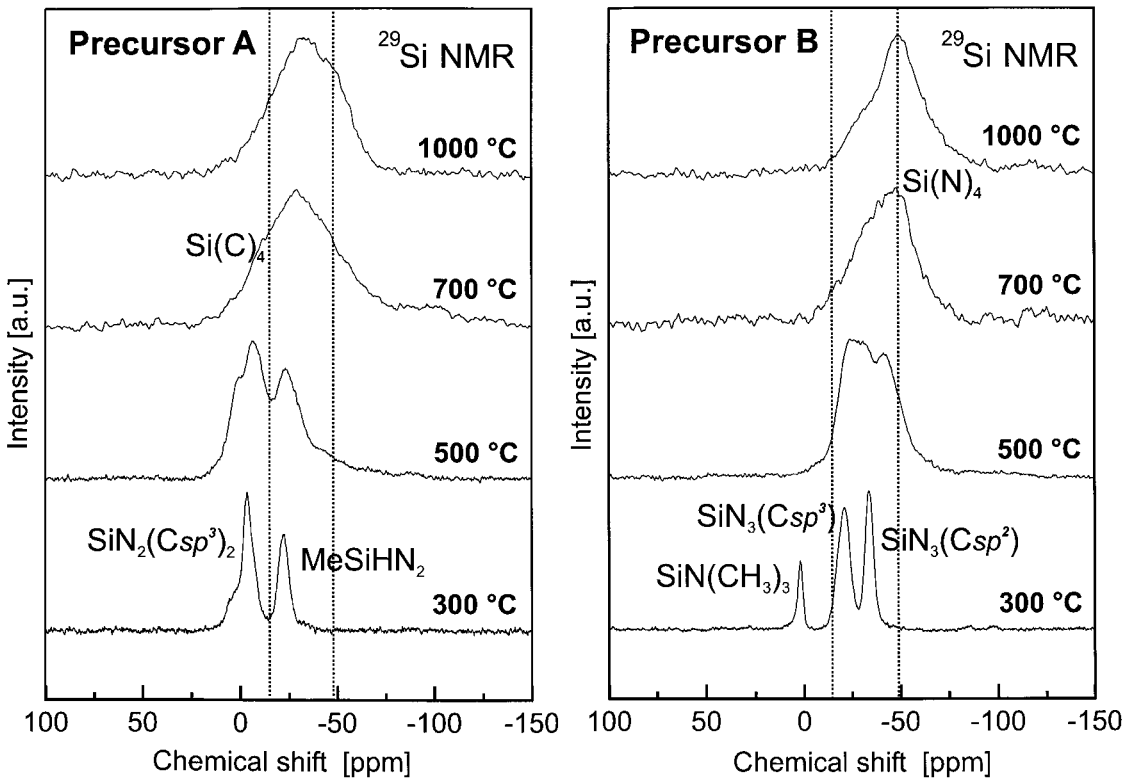

Figure 1 ^{29}Si NMR spectra of precursor A and B powder samples annealed between 300 and 1000 °C. Note that precursor A forms predominantly SiN_xC_y mixed units, whereas precursor B reveals a high volume fraction of Si—N bonding.

Ball milling (Teflon container, ZrO_2 milling balls) and sieving of the cross-linked polymer yielded a polymer powder $\leq$32 μm, which was blended with 30 vol% of the starting liquid precursor. Possible contamination during powder processing was not observed (chemical, in addition to TEM energy-dispersive X-ray (EDX), analysis). The added liquid precursor acts both as a filler and as a reactive component that coalesces with the powder particles. Uniaxial die pressing at 10 MPa and 120–140 °C resulted in a powder compact ($70 \times 6 \times 4$ mm^2) of about 75% green density of the polymer powder. Subsequent annealing at 1000 °C for 1 h in nitrogen yielded amorphous SiCN monoliths (see Fig. 1). Subsequent annealing at temperatures ranging from 1400 to 1540 °C in a nitrogen atmosphere with varying holding times was applied to study the effect of heat treatment on crystallization.

Microstructure characterization of the polymer-derived materials after pyrolysis and subsequent annealing was performed by scanning electron microscopy (SEM), using a JEOL 6400 microscope, equipped with an ultrathin window germanium EDX detector, as well as by TEM utilizing a Philips CM20FEG (field emission gun) microscope, which was also equipped with an EDX system and an electron energy-loss spectrometer with parallel detection (PEELS, Gatan 666). Energy resolution during spectra acquisition was 0.8 eV with an energy dispersion of 0.1 eV. TEM-foil preparation followed standard techniques, which involve diamond cutting, ultrasound drilling, mechanical grinding, dimpling, argon-ion thinning to perforation and subsequent light carbon coating to minimize electrostatic charging under the electron beam.

3 RESULTS AND DISCUSSION

The general idea of using polymer powders derived from organometallic polymers with different struc-

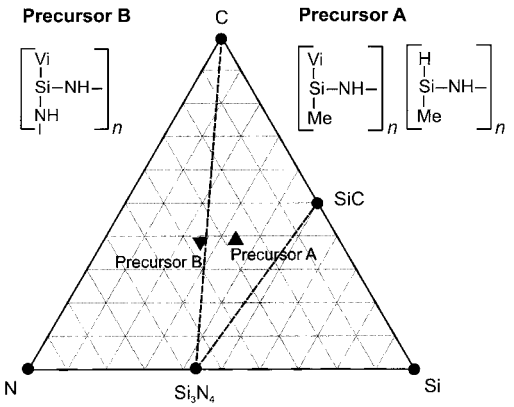

Figure 2 Structural units of the two precursors used and their corresponding positions within the ternary phase diagram Si–C–N.

tural units was based on the assumption that the resulting amorphous material will be affected by the intrinsic architecture of the starting polymer. The goal of the present study was to gain insight to what extent the thermal stability of the polymer-derived glass structure, which is synonymous with the respective crystallization behavior and the resulting overall microstructure evolution, is influenced by the polymer architecture and/or the chemical composition of the precursor used. It should be noted here that the two precursors studied have different compositions, with precursor B being carbon rich (see the Si–C–N phase diagram in Fig. 2). In the following we use the argument that the architecture, i.e. the polymer-derived glass structure, is, in principle, based on the respective silicon network. To support this argument, Fig. 1 shows the variation of the ^{29}Si NMR signal upon heat treatment between 300 and 1000 °C. It is shown that the network of precursor B is dominated by Si—N bonding, whereas precursor A reveals predominantly Si—N_x—C_y mixed units. This indicates that we can distinguish between the silicon-based network and — as will be discussed later — the carbon phase that is incorporated (precursor A) or builds up a separate interpenetrating carbon network (precursor B).

Figure 2 depicts the structural units of the different precursors used and the positions of the different polymer-derived materials within the ternary phase diagram after exposure at 1000 °C for 1 h in a nitrogen atmosphere, as acquired by chemical analysis. As can be seen, the sample obtained from precursor A is located within the compatibility triangle of the thermodynamically stable phases SiC, Si_3N_4 and C, whereas the sample prepared with precursor B is almost placed on the tie line Si_3N_4–C, but slightly outside the compatibility triangle of precursor A.

Based on earlier investigations, the amorphous state of polymer-derived ceramics within the Si–C–N system after pyrolysis at 1000 °C can be described as a continuous network of various mixed Si—C_x—N_y environments plus a free carbon phase, as revealed by NMR and Raman experiments[44,45] (Fig. 3). Exposure to temperatures exceeding 1000 °C promotes rearrangements within the amorphous network. From chemical analysis data (given in Table 1) it is concluded that these local rearrangements are solely structural, since no significant compositional changes were monitored upon annealing. Thermogravimetric analysis confirmed this observation. Structural reorganization leads to the formation of SiN_4 short-range ordered areas, as demonstrated by NMR experiments, in addition to the presence of a free carbon phase, as shown by Raman spectroscopy (Fig. 4). The two Raman bands centered at 1280 and 1600 cm^{-1} are allocated to the D and G bands respectively, and are the two most prominent features of disordered graphitic carbon. This obviously indicates carbon segregation to form disordered or nanocrystalline graphitic clusters. Since line width decreases with increasing pyrolysis temperature, structural rearrangements accompanied by ordering and/or growth of the free carbon phase occur in the temperature range between 1400 and 1540 °C.

In order to gain further information on the overall microstructure development during high-temperature annealing, electron microscopy was applied as a complementary characterization technique. Figure 5 shows SEM images of fracture surfaces of precursor A- and B-derived materials annealed at 1540 °C. As can be seen, both materials exhibited residual open porosity of about 15 vol%, but showed an overall homogeneous microstructure with no indication of local crystallization. Despite residual porosity, the materials contain dense regions, which are considered here as the monolithic bulk material of the corresponding Si–C–N system. Only these bulk regions were characterized to study crystallization behavior and thermal stability of the associated glass systems. It is true that the residual porosity cannot simply be neglected when discussing crystallization phenomena in such non-oxide glass systems. Earlier we reported on the possible effect of nanoporosity[40,41] initiating devitrification. However, here we focus on the behavior of dense regions to understand the

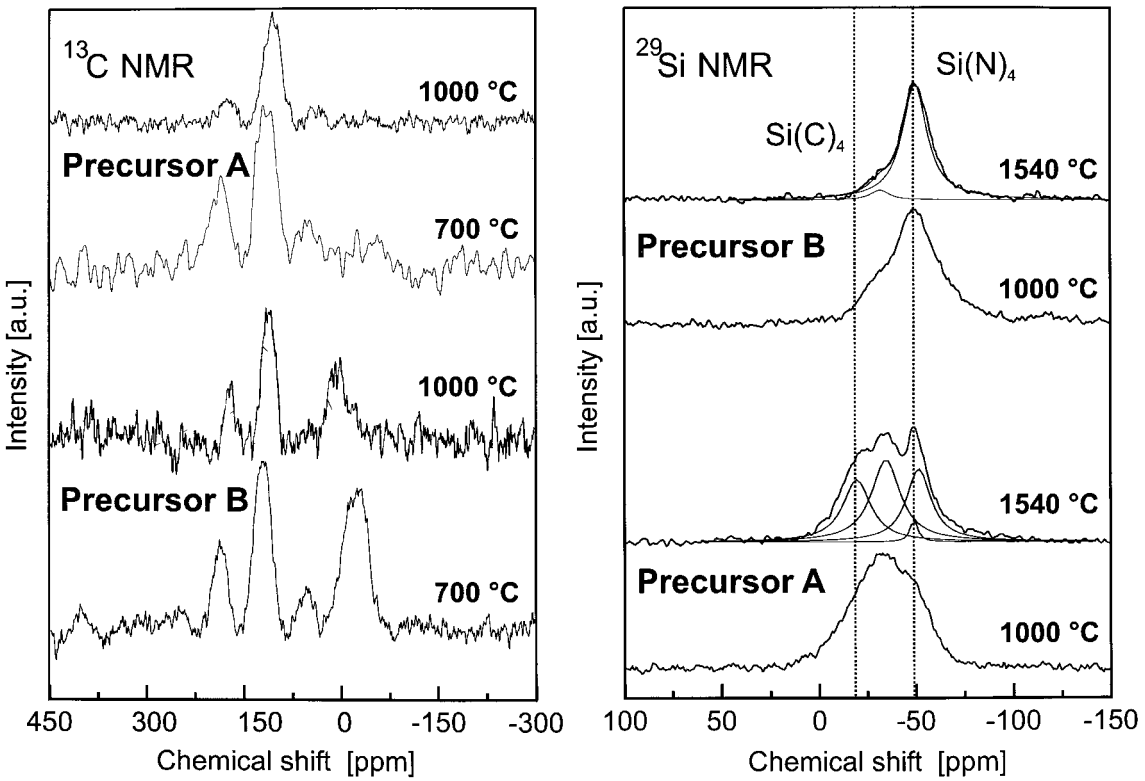

Figure 3 ^{13}C NMR spectra of precursor A- and B-derived powder samples heat treated at 700 and 1000 °C and ^{29}Si NMR spectra of precursor A and B powder samples annealed at 1000 and 1500 °C (deconvoluted). The dashed lines indicate the SiC_4 and the SiN_4 signals.

basic mechanism effective in the bulk Si–C–N system.

Upon pyrolysis at 1000 °C, both polymer-derived SiCN materials were electronoptically amorphous, revealing a diffuse elastically scattered ring pattern during selected-area diffraction (SAD). Utilizing TEM, microstructure characterization of material A, annealed at 1540 °C/6 h/nitrogen, revealed the formation of large α-Si_3N_4 crystallites (2–5 μm) within the overall amorphous SiCN structure, as shown in Fig. 6(a). Moreover, applying high-resolution TEM (HRTEM) imaging, it was revealed that the bulk of this material was in fact not completely amorphous but showed in some

Table 1 Chemical analysis of ceramic residues pyrolyzed at 1000 and 1540 °C

	Composition (wt %)						
Precursor	Si	N	C	H	O	SiCN stoichiometry	C_{free} (mol %)
A							
1000 °C	51.4	21.9	25.5	<0.1	0.4	$SiN_{0.85}C_{0.36} + 0.80C$	26.0
1540 °C	52.0	23.0	25.1	<0.1	0.4	$SiN_{0.89}C_{0.33} + 0.80C$	26.0
B							
1000 °C	42.5	30.8	25.6	<0.1	0.8	$SiN_{1.33} + 1.41C + 0.12N$	35.6
1540 °C	43.4	29.1	26.3	<0.1	0.8	$SiN_{1.33} + 1.42C + 0.02N$	37.0

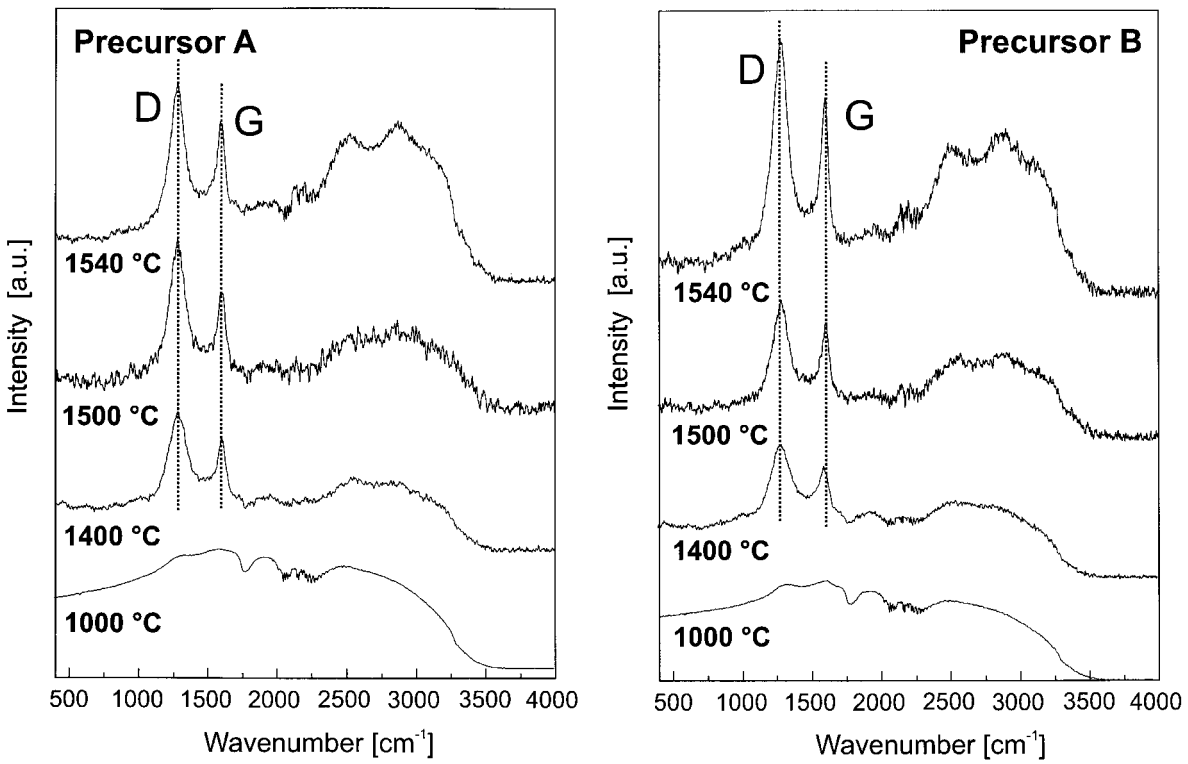

Figure 4 Raman spectra of pyrolytic residues annealed at temperatures between 1000 and 1550 °C. The dashed lines indicate the D and G bands.

areas the formation of SiC nuclei. Nevertheless, it should be emphasized that the majority of the material remained amorphous, with no indication of phase separation into amorphous silicon nitride and disordered graphitic areas, as suggested by Raman spectroscopy (see Fig. 4). Examining material B, no difference in microstructure after high-temperature annealing at 1540 °C/6 h/nitrogen (Fig. 6(b)), compared with the material pyrolyzed at 1000 °C, could be established. Pure phase contrast, typical for thin amorphous materials, is seen when imaging at high resolution. Also, no indication for phase separation or local crystallization was observed, although this material has a significantly higher content of free carbon (see also Table 1).

In addition to HRTEM imaging of the amorphous phase, energy loss near edge structure (ELNES) studies of the Si-$L_{2,3}$, C-K and N-K ionization edges were performed at the very same regions of HRTEM image recording, in order to characterize the local chemical environment within the Si–C–N matrix. Figure 7 shows two ELNES spectra of the C-K edge taken within materials A and B after exposure at 1400 °C. It should be noted that the corresponding ELNES spectra of the Si-$L_{2,3}$ (100 eV) and N-K (401 eV) edges showed no marked difference. Only the C-K edge indicated two distinct carbon surroundings, namely amorphous carbon and graphitic carbon. Corresponding HRTEM imaging given in Fig. 8, in addition to electron diffraction, revealed in all cases a homogeneous microstructure with no clear indication of large isolated graphite precipitates. However, it should be noted that the free carbon, which was clearly detected by Raman spectroscopy, is expected to be present in regions of $\leq$1–2 nm. Since these small disordered clusters are embedded within an amorphous matrix, direct imaging becomes rather difficult. Moreover, it can be concluded that the scale of a possible phase separation monitored by NMR spectroscopy (see also Fig. 3) into free carbon, amorphous Si_3N_4 and mixed Si—C_x—N_y tetrahedra within material A and, on the other hand, into amorphous Si_3N_4 and

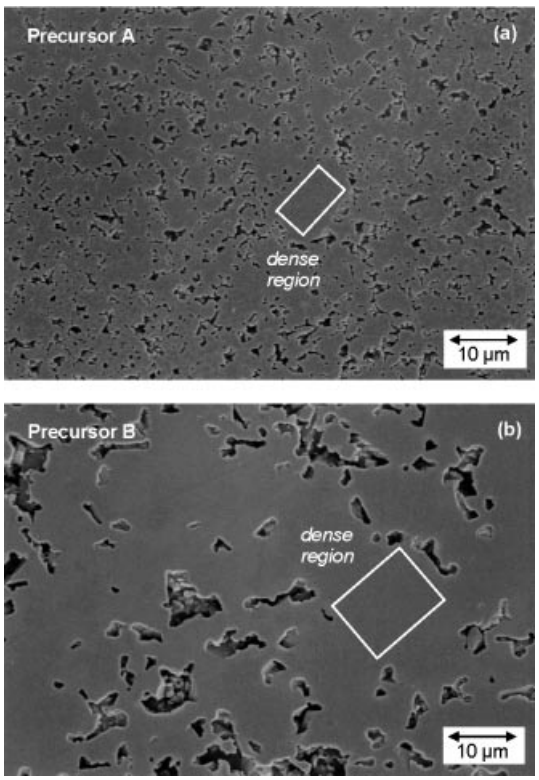

Figure 5 SEM micrographs of the fracture surface of (a) sample A after annealing at 1540 °C/6 h/nitrogen and (b) sample B annealed under the same conditions.

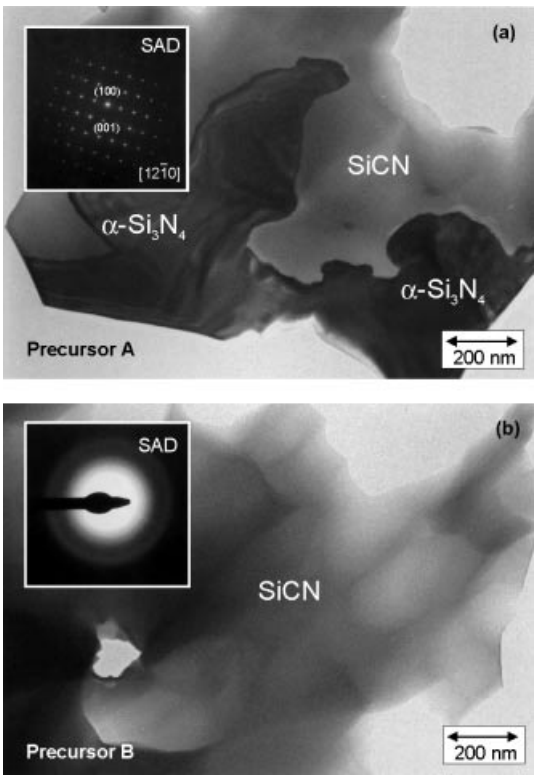

Figure 6 TEM micrographs of (a) material A after heat treatment at 1540 °C/6 h/nitrogen. Despite the formation of large α-Si_3N_4 crystallites (2–5 µm), the overall microstructure of the material remained amorphous. (b) Material B annealed at 1540 °C/6 h/nitrogen. Note that no local precipitation/crystallization was observed in this sample.

graphitic carbon in material B, is in most cases reduced to the size of a few BSUs. Structural/chemical variations at such length scales are hardly accessible even when imaged at high resolution (HRTEM). Although the actual reason for the obvious difference in high-temperature response (local crystallization in material A, and high-temperature resistance of material B) is not yet known, it is assumed here that the higher free carbon content of material B is responsible for the unexpected stability of the amorphous matrix. Based on NMR in conjunction with HRTEM results, it is concluded that the thermal stability is governed by the intrinsic silicon network, i.e. the incorporation of carbon into the glass structure. In material B we observed numerous turbostratic carbon precipitates (1–2 nm) by HRTEM imaging (see Fig. 8(b)), which is consistent with the NMR data emphasizing pronounced Si—N bonding. In contrast, polymer A, which is composed of different structural units, favors the incorporation of carbon into the silicon backbone structure. For example, structural rearrangements at 1400 °C create SiN_4 and SiC_4 environments that, when larger than a critical nucleus radius, promote local crystallization. SiN_4 units are predominantly present in glass B (see Fig. 1). As carbon is not incorporated into the structure (Si-backbone) of glass B (or is only present in a small fraction), the free carbon is consequently finely dispersed within the matrix. This configuration, in turn, acts as a diffusion barrier, similar to B(C)N formation in Si–B–C–N ceramics,[42] restricting local crystallization.

4 CONCLUSIONS

The amorphous state of polymer-derived ceramics

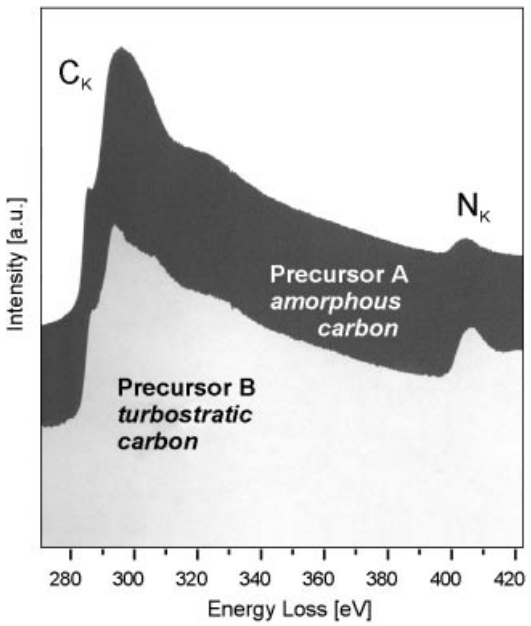

Figure 7 ELNES spectra of the ionization C-K edge taken within different regions of the amorphous matrix of material A after exposure at 1400 °C. Two different carbon surroundings were observed, namely amorphous (top) and graphitic (bottom).

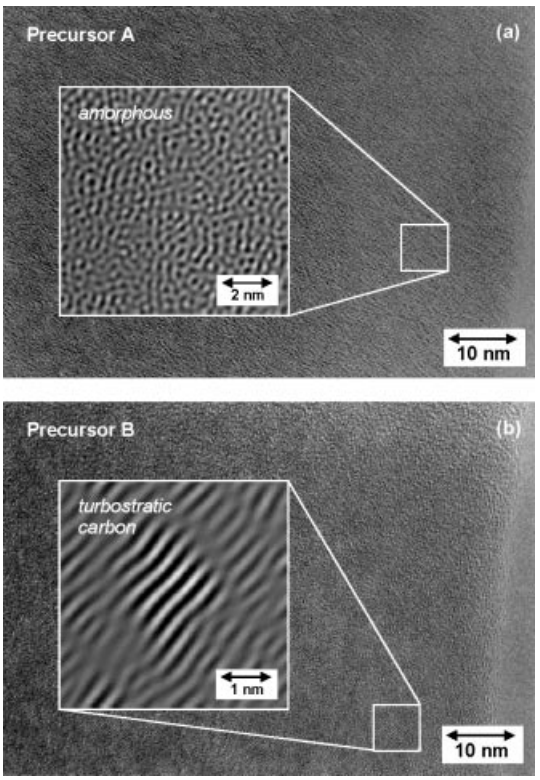

Figure 8 HRTEM micrographs of (a) material A and (b) material B, both of which correspond to the different ELNES spectra of the C-K ionization edge given in Fig. 7.

within the Si–C–N system after pyrolysis at 1000 °C typically consists of various mixed Si—C_x—N_y environments in addition to a free carbon phase, as revealed by NMR and Raman experiments. Exposure to temperatures exceeding 1000 °C promotes structural rearrangements of the amorphous network with negligible changes in chemical composition (depletion of nitrogen). This results in the formation of disordered SiC_4 and SiN_4 areas next to a free carbon phase.

TEM characterization upon high-temperature annealing clearly revealed different crystallization behavior depending on the polymer used. In the precursor A-derived material, large α-Si_3N_4 crystallites (2–5 μm) and a small number of SiC precipitates (10–20 nm) were observed. However, material B remained completely amorphous up to 1540 °C. The reason for the obvious difference in high-temperature response, i.e. the local crystallization within material A in contrast to the high-temperature resistance of glass B, is due to the different silicon-based glass networks evolved during synthesis/annealing. Carbon was incorporated into the structure of precursor A, whereas in material B it was not (or only to a small volume fraction). Structural rearrangement at elevated temperatures formed SiN_4 and SiC_4 environments in glass A, which is prone to crystallize. Since carbon is not incorporated into the B-glass structure, the resulting fine dispersion of carbon (nanometer range) acts as a diffusion barrier (similar to a B(C)N formation) restricting local crystallization. Hence, although two precursors with different chemical compositions were analyzed, their intrinsic polymer architecture/glass structure is responsible for the respective crystallization behavior. Carbon incorporation combined with local structural rearrangements within the silicon network favor crystallization. On the other hand, the occurrence of two separated interpenetrating networks (Si–N and C–C) — like in precursor B — improves the thermal stability of the Si–C–N ceramic.

Acknowledgements The authors would like to express their thanks to the Volkswagenstiftung Hannover and the Deutsche

Forschungsgemeinschaft (DFG) Bonn for financial support throughout the work.

REFERENCES

1. Verbeek W and Winter G. *Ger. Offen*. 2 236 078, 21 March, 1974, Bayer AG, Leverkusen, Germany.
2. Yajima S, Hayashi J, Omori M and Okamura K. *Nature* 1976; **261**: 683.
3. Seyferth D and Wiseman GH. *J. Am. Ceram. Soc.* 1984; **67**(7): C132.
4. Birot M, Pillot J-P and Dunoguès J. *Chem. Rev.* 1995; **95**: 1443.
5. Narisawa M, Okamura K, Sugimoto K and Seguchi T. *Bull. Chem. Soc. Jpn.* 1995; **68**: 1098.
6. Laine RM, Blum YD, Tse D and Glaser R. Synthetic routes to oligosilazanes and polysilazanes. In *Inorganic and Organometallic Polymers*. American Chemical Society: 1988; Chapter 10.
7. Lücke J, Hacker J, Suttor D and Ziegler G. *Appl. Organomet. Chem.* 1997; **11**: 181.
8. Hapke J and Ziegler G. *Adv. Mater.* 1995; **7**(4): 380.
9. Riedel R, Bill J and Kienzle A. *Appl. Organomet. Chem.* 1996; **10**: 241.
10. Baldus H-P, Jansen M and Wagner O. *Key Eng. Mater.* 1994; **89–91**: 75.
11. Richter R et al. *Appl. Organomet. Chem.* 1997; **11**: 71.
12. Sartori P and Habel W. *J. Prakt. Chem.* 1996; **338**: 197.
13. Hacker J, Motz G and Ziegler G. Entwicklung maßgeschneiderter Si(CN)-Polymere. In *Proc. Werkstoffwoche München*, Heinrich J, Ziegler G, Hermel W, Riedel H (eds). Wiley–VCH: Weinheim, 1999; 303–308.
14. Vaahs T, Brück M and Böcker WDG. *Adv. Mater.* 1992; **4**: 224.
15. Schwartz KB, Rowcliffe DJ and Blum YD. *Adv. Ceram. Mater.* 1988; **3**(4): 320.
16. Ziegler G, Hapke J and Lücke J. *Ceram. Trans.* 1995; **58**(2): 13.
17. Niihara K. *J. Ceram. Soc. Jpn.* 1991; **99**: 974.
18. Riedel R, Kleebe H-J, Schönfelder H and Aldinger F. *Nature* 1995; **374**: 526.
19. Boden G, Neumann A, Breuning T, Tschernikova E and Hermel W. *J. Eur. Ceram. Soc.* 1998; **18**: 1461.
20. Bill J and Heimann D. *J. Eur. Ceram. Soc.* 1996; **16**: 1115.
21. Passing G, Schönfelder H, Riedel R and Brook RJ. *Br. Ceram. Trans.* 1993; **92**(1): 21.
22. Gonon MF, Fantozzi G, Murat M and Disson JP. *J. Eur. Ceram. Soc.* 1995; **15**: 591.
23. Riedel R, Passing G, Schönfelder H and Brook RJ. *Nature* 1992; **355**: 714.
24. Choong Kwet Yive NS, Corriu RJP, Leclercq D, Mutin PH and Vioux A. *Chem. Mater.* 1992; **4**: 141.
25. Choong Kwet Yive NS, Corriu RJP, Leclercq D, Mutin PH and Vioux A. *Chem. Mater.* 1992; **4**: 1263.
26. Bahloul D, Pereira M and Gerardin C. *J. Mater. Chem.* 1997; **7**(1): 109.
27. Laine RM, Babonneau F, Blowhowiak KY, Kennish RA, Rahn JA, Exarhos GJ and Waldner K. *J. Am. Ceram. Soc.* 1995; **78**(1): 137.
28. Seitz J, Bill J, Egger N and Aldinger F. *J. Eur. Ceram. Soc.* 1996; **16**: 885.
29. Dando NR, Perrotta AJ, Strohmann C, Steward RM and Seyferth D. *Chem. Mater.* 1993; **5**: 1624.
30. Blum YD, Schwartz KB and Laine RM. *J. Mater. Sci.* 1989; **24**: 1707.
31. Gerardin C, Taulelle F and Bahloul D. *J. Mater. Chem.* 1997; **7**(1): 117.
32. Dixmier J, Belissent R, Bahloul D and Goursat P. *J. Eur. Ceram. Soc.* 1994; **13**: 293.
33. Schempp S, Dürr J, Lamparter P, Bill J and Aldinger F. *Z. Naturforsch. Teil A* 1998; **53**: 127.
34. Ténégal F, Bouchet B, Bellissent R, Herlin N, Cauchetier M and Dixmier J. *Philos. Mag. A* 1998; **78**(4): 803.
35. Monthioux M and Delverdier O. *J. Eur. Ceram. Soc.* 1996; **16**: 721.
36. Ziegler G, Kleebe H-J, Motz G, Müller H, Weibelzahl W and Traßl S. *J. Mater. Chem. Phys.* 1999; **61**: 55.
37. Haluschka C, Engel C and Riedel R. *J. Eur. Ceram. Soc.* 2000; **20**: 1365.
38. Nishimura T, Haug R, Bill J, Thurn G and Aldinger F. *J. Mater. Sci.* 1998; **33**: 5237.
39. Delverdier O, Monthioux M, Oberlin A, Lavedrine A, Bahloul D and Goursat P. *High Temp. Chem. Process.* 1992; **1**: 139.
40. Kleebe H-J. *Phys. Statis. Solid A* 1998; **166**: 297.
41. Kleebe H-J, Suttor D, Müller H and Ziegler G. *J. Am. Ceram. Soc.* 1998; **81**(11): 2971.
42. Bill J, Aldinger F. *Adv. Mater.* 1995; **7**(9): 775.
43. Kleebe H-J, Braue W, Schmidt H, Pezzotti G and Ziegler G. *J. Eur. Ceram. Soc.* 1996; **16**: 339.
44. Trassl S, Suttor D, Motz G, Rößler E and Ziegler G. *J. Eur. Ceram. Soc.* 2000; **20**: 215.
45. Traßl S, Suttor D, Motz G, Rößler E and Ziegler G. *J. Eur. Ceram. Soc.* 2000; **20**: 215.

